Echocardiography

in Pediatric and Congenital Heart Disease

From Fetus to Adult

Edited by Wyman W. Lai, Luc L. Mertens
Meryl S. Cohen, Tal Geva

SECOND EDITION

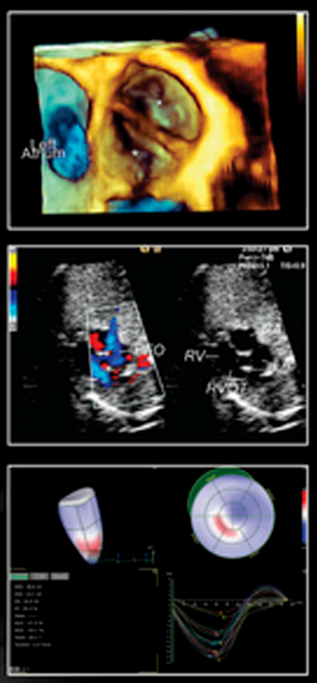

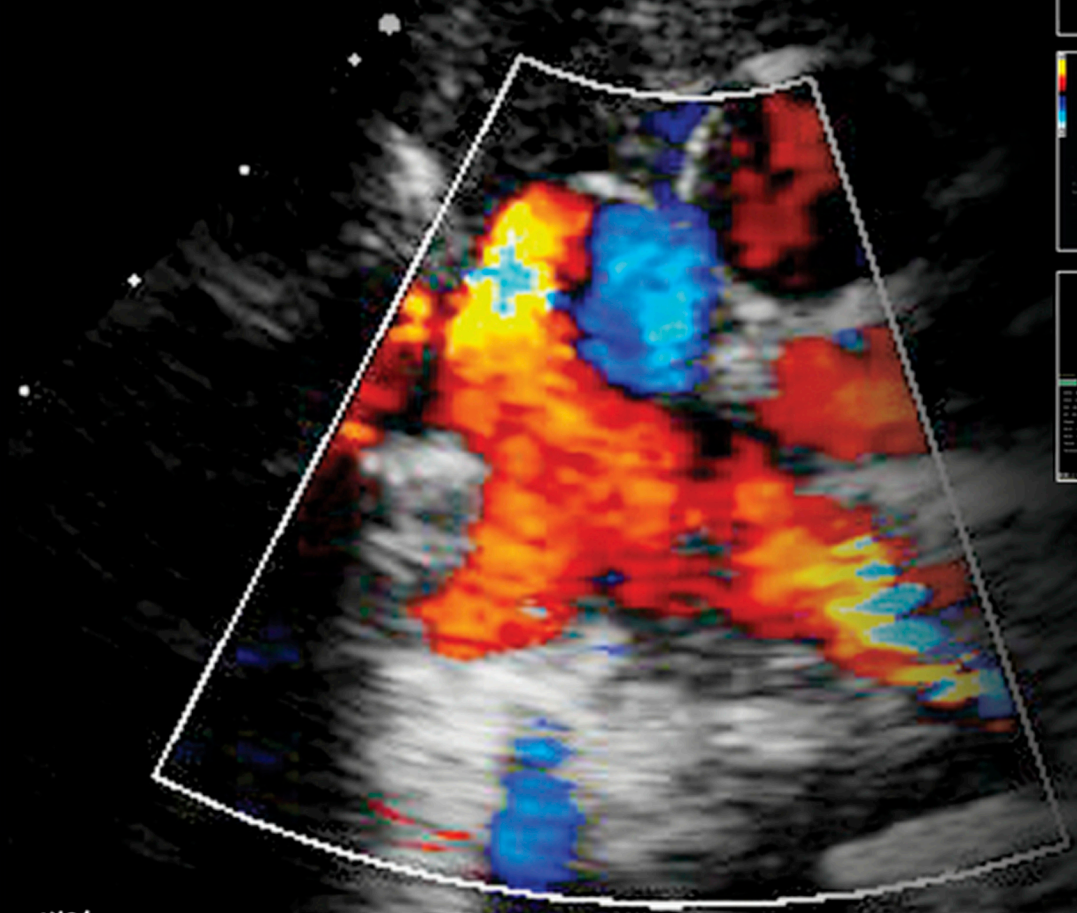

with website

WILEY Blackwell

Echocardiography in Pediatric and Congenital Heart Disease

Dedications

To my parents, CheToo and SoFa Lai; my wonderful wife, Lydia; and my children, Justin and Amanda.

Wyman W. Lai

To my wife Benedikte, my daughter Virginie and my son Francis. For all the time I could not spend with them.

Luc L. Mertens

To my husband Bruce Randazzo and my children Jake, Isabel and Ethan for supporting me always.

Meryl S. Cohen

To my wife Judith and sons Omri and Alon with Love.

Tal Geva

Echocardiography in Pediatric and Congenital Heart Disease

From Fetus to Adult

Second Edition

Edited by

Wyman W. Lai MD, MPH

Professor of Pediatrics at CUMC
Columbia University Medical Center;
Director, Noninvasive Cardiac Imaging
Morgan Stanley Children's Hospital of NewYork-Presbyterian
New York, NY, USA

Luc L. Mertens MD, PhD

Section Head, Echocardiography
The Hospital for Sick Children;
Professor of Pediatrics
University of Toronto
Toronto, ON, Canada

Meryl S. Cohen MD

Professor of Pediatrics
Perelman School of Medicine, University of Pennsylvania;
Medical Director, Echocardiography
Program Director, Cardiology Fellowship
The Cardiac Center
The Children's Hospital of Philadelphia
Philadelphia, PA, USA

Tal Geva MD

Professor of Pediatrics
Harvard Medical School;
Chief, Division of Noninvasive Cardiac Imaging
Department of Cardiology
Boston Children's Hospital
Boston, MA, USA

WILEY Blackwell

This edition first published 2016 © 2016 by John Wiley & Sons Ltd.
First edition published 2009 © 2009 by John Wiley & Sons Ltd.

Registered office: John Wiley & Sons, Ltd, The Atrium, Southern Gate, Chichester, West Sussex, PO19 8SQ, UK

Editorial offices: 9600 Garsington Road, Oxford, OX4 2DQ, UK
The Atrium, Southern Gate, Chichester, West Sussex, PO19 8SQ, UK
111 River Street, Hoboken, NJ 07030-5774, USA

For details of our global editorial offices, for customer services and for information about how to apply for permission to reuse the copyright material in this book please see our website at www.wiley.com/wiley-blackwell

Library of Congress Cataloging-in-Publication Data

Echocardiography in pediatric and congenital heart disease : from fetus to adult / edited by Wyman W. Lai, Luc L. Mertens, Meryl S. Cohen, Tal Geva. – Second edition.
p. ; cm.
Includes bibliographical references and index.
ISBN 978-0-470-67464-2 (cloth)
I. Lai, Wyman W., editor. II. Mertens, Luc, editor. III. Cohen, Meryl, editor. IV. Geva, Tal, editor.
[DNLM: 1. Heart Defects, Congenital–ultrasonography. 2. Echocardiography–methods. 3. Heart Defects, Congenital–diagnosis. WG 141.5.E2]
RJ423.5.U46
618.92′1207543–dc23

2015033801

A catalogue record for this book is available from the British Library.

Wiley also publishes its books in a variety of electronic formats. Some content that appears in print may not be available in electronic books.

Cover images: Reproduced from images within the book.

Set in 9.5/12pt MinionPro by Aptara Inc., New Delhi, India

1 2016

Contents

Contributors

Vivekanand Allada MD
Professor of Pediatrics
University of Pittsburgh School of Medicine
Director of Clinical Services, Pediatric Cardiology
Children's Hospital of Pittsburgh of UPMC
Heart Institute
Pittsburgh, PA, USA

Bhawna Arya MD
Assistant Professor
Department of Pediatrics
University of Washington School of Medicine
Seattle Children's Hospital
Seattle, WA, USA

Piers C.A. Barker MD
Associate Professor of Pediatrics and Obstetrics/Gynecology
Duke University Medical Center
Durham, NC, USA

Aaron J. Bell MD
Department of Congenital Heart Disease
Evelina London Children's Hospital;
Guy's & St Thomas' NHS Foundation Trust
London UK

Rebecca S. Beroukhim MD
Director, Fetal Echocardiography
Instructor in Pediatrics
Massachusetts General Hospital
Boston, MA, USA

William L. Border MBChB, MPH, FASE
Director of Noninvasive Cardiac Imaging
Medical Director, Cardiovascular Imaging Research Core (CIRC)
Children's Healthcare of Atlanta Sibley Heart Center;
Associate Professor
Emory University School of Medicine
Atlanta, GA, USA

David W. Brown MD
Assistant Professor of Pediatrics
Department of Cardiology
Boston Children's Hospital;
Department of Pediatrics
Harvard Medical School
Boston, MA, USA

Frank Cetta MD
Professor of Medicine and Pediatrics
Mayo Clinic
Rochester, MN, USA

Sarah Chambers MD
The Pediatric Heart Center at the Children's Hospital at Montefiore
New York, NY, USA

Michael Cheung BSc, MB ChB, MRCP(UK), MD
Associate Professor
Head of Cardiology
Royal Children's Hospital;
Department of Paediatrics
University of Melbourne;
Heart Research Group
Murdoch Childrens Research Institute
Melbourne, VIC, Australia

Meryl S. Cohen MD
Professor of Pediatrics
Perelman School of Medicine, University of Pennsylvania;
Medical Director, Echocardiography
Program Director, Cardiology Fellowship
The Cardiac Center
The Children's Hospital of Philadelphia
Philadelphia, PA, USA

Steven D. Colan MD
Professor of Pediatrics
Harvard Medical School;
Boston Children's Hospital
Boston, MA, USA

Julie De Backer MD, PhD
Senior Lecturer
Department of Cardiology and Medical Genetics
University Hospital Ghent
Ghent, Belgium

Jan D'hooge MD
Professor
Department of Cardiovascular Sciences
Catholic University of Leuven;
Medical Imaging Research Center
University Hospital Gasthuisberg
Leuven, Belgium

Allison Divanovic MD
Assistant Professor of Pediatrics
University of Cincinnati College of Medicine
The Heart Institute
Cincinnati Children's Hospital Medical Center
Cincinnati, OH, USA

Stacey Drant MD
Associate Clinical Professor
Director, Pediatric Echocardiography Laboratory
Children's Hospital of Pittsburgh
Pittsburgh, PA, USA

Benjamin W. Eidem MD, FACC, FASE
Professor of Pediatrics and Medicine
Mayo Clinic
Rochester, MN, USA

Matthew Fenton MB, BS, BSc
Consultant Paediatric Cardiologist
Cardiothoracic Unit
Great Ormond Street Hospital for Children and Institute of Cardiovascular Sciences
London, UK

Mark K. Friedberg MD
Associate Professor of Pediatrics
The Labatt Family Heart Center
The Hospital for Sick Children
University of Toronto
Toronto, ON, Canada

Peter C. Frommelt MD
Professor of Pediatrics
Director of Echocardiography
Division of Pediatric Cardiology
Medical College of Wisconsin
Children's Hospital of Wisconsin
Milwaukee, WI, USA

Michele A. Frommelt MD
Associate Professor of Pediatrics
Children's Hospital of Wisconsin
Milwaukee, WI, USA

Javiar Ganame MD, PhD
Department of Medicine
Division of Cardiology
McMaster University
Hamilton, ON, Canada

Tal Geva MD
Professor of Pediatrics
Harvard Medical School;
Chief, Division of Noninvasive Cardiac Imaging
Department of Cardiology
Boston Children's Hospital
Boston, MA, USA

Marc Gewillig MD, PhD, FESC, FACC, FSCAI
Professor Paediatric & Congenital Cardiology
University Hospitals Leuven
Leuven, Belgium

David J. Goldberg MD
Assistant Professor
Division of Pediatric Cardiology
The Children's Hospital of Philadelphia;
Perelman School of Medicine, University of Pennsylvania
Philadelphia, PA USA

J. René Herlong MD
Associate Clinical Professor of Pediatric Cardiology
Sanger Heart and Vascular Institute
Levine Children's Hospital
Charlotte, NC, USA

Lisa K. Hornberger MD
Professor of Pediatrics and Obstetrics & Gynecology
Director, Fetal and Neonatal Cardiology Program
Section Head, Pediatric Echocardiography
Stollery Children's Hospital
Edmonton, AB, Canada

Darren P. Hutchinson MBBS, FRACP
Fetal & Pediatric Cardiologist
Department of Pediatric Cardiology
The Royal Children's Hospital
Melbourne, VIC, Australia

Sachin Khambadkone MD
Paediatric and Adolescent Cardiology, Interventional Cardiologist
Great Ormond Street Hospital for Children and Institute of Cardiovascular Sciences
London, UK

Mary Etta E. King MD
Associate Professor of Pediatrics
Massachusetts General Hospital
Boston, MA, USA

H. Helen Ko BS, RDMS, RDCS
Mount Sinai Medical Center
New York, NY, USA

Joe R. Kreeger RCCS, RDCS
Technical Director, Echocardiography
Children's Healthcare of Atlanta Sibley Heart Center
Atlanta, GA, USA

Andreas Kühn MD
Department of Pediatric Cardiology and Congenital Heart Disease
Deutsches Herzzentrum München
Technische Universität München
Munich, Germany

Wyman W. Lai MD, MPH
Professor of Pediatrics at CUMC
Columbia University Medical Center;
Director, Noninvasive Cardiac Imaging
Morgan Stanley Children's Hospital of NewYork-Presbyterian
New York, NY, USA

Matthew S. Lemler MD
Professor of Pediatrics
Division of Cardiology
University of Texas Southwestern;
Director, Echocardiography Laboratory
Children's Medical Center of Dallas
Dallas, TX, USA

Jami C. Levine MS, MD
Associate in Cardiology
Assistant Professor of Pediatrics
Boston Children's Hospital
Boston, MA, USA

Leo Lopez MD
Associate Professor of Clinical Pediatrics
The Pediatric Heart Center
Children's Hospital at Montefiore
New York, NY, USA

Irene D. Lytrivi MD
Assistant Professor of Pediatrics
Icahn School of Medicine at Mount Sinai
Division of Pediatric Cardiology
Mount Sinai Medical Center
New York, NY, USA

Jan Marek MD, PhD
Associate Professor of Cardiology
Institute of Child Health
University College London;
Director of Echocardiography
Consultant Pediatric and Fetal Cardiologist
Great Ormond Street Hospital for Children
London, UK

Renee Margossian MD
Assistant Professor of Pediatrics
Harvard Medical School
Department of Cardiology
Boston Children's Hospital
Boston, MA, USA

Jackie McGhie
Congenital Cardiac Ultrasound Specialist
Department of Cardiology
Erasmus University Rotterdam
Rotterdam, The Netherlands

Colin J. McMahon MB, BCh, FRCPI, FAAP
Consultant Paediatric Cardiologist
Department of Paediatric Cardiology
Our Lady's Hospital for Sick Children
Crumlin, Ireland

Folkert Jan Meijboom MD, PhD
Staff Physician
Department of Pediatrics and Cardiology
Academic Medical Centre Utrecht
Utrecht, The Netherlands

Luc L. Mertens MD, PhD
Section Head, Echocardiography
The Hospital for Sick Children;
Professor of Pediatrics
University of Toronto
Toronto, ON, Canada

Erik C. Michelfelder MD
Associate Professor of Pediatrics
University of Cincinnati College of Medicine
The Heart Institute
Cincinnati Children's Hospital Medical Center
Cincinnati, OH, USA

Owen I. Miller FRACP, FCSANZ, FRCPCH
Head of Service/Clinical Lead, Congenital Heart Disease
Consultant in Pediatric and Fetal Cardiology
Evelina London Children's Hospital;
Guy's & St Thomas' NHS Foundation Trust;
Honorary Senior Lecturer, Kings College London
London, UK

Shobha Natarajan MD
Assistant Professor of Clinical Pediatrics
The University of Pennsylvania School of Medicine
Division of Cardiology
The Children's Hospital of Philadelphia
Philadelphia, PA, USA

James C. Nielsen MD
Associate Professor of Pediatrics and Radiology
Chief, Division of Pediatric Cardiology
Stony Brook Children's
Stony Brook, NY, USA

Erwin Oechslin MD, FRCPC, FESC
Director, Toronto Congenital Cardiac Centre for Adults
The Bitove Family Professor of Adult Congenital Heart Disease;
Professor of Medicine, University of Toronto
Peter Munk Cardiac Centre
University Health Network/Toronto General Hospital
Toronto, ON, Canada

Laurie E. Panesar MD
Assistant Professor of Pediatrics
Director, Fetal and Pediatric Echocardiography
Stony Brook Children's
Stony Brook, NY, USA

Ira A. Parness MD
Professor of Pediatrics
Division of Pediatric Cardiology
Mount Sinai Medical Center
New York, NY, USA

Andrew J. Powell MD
Department of Cardiology, Boston Children's Hospital;
Associate Professor of Pediatrics
Department of Pediatrics, Harvard Medical School
Boston, MA, USA

Claudio Ramaciotti MD
Professor of Pediatrics
Division of Cardiology
University of Texas Southwestern;
Children's Medical Center of Dallas
Dallas, TX, USA

Bo Remenyi MD
Menzies School of Health Research
Charles Darwin University
Darwin, NT, Australia

Jack Rychik MD
Professor of Pediatrics
Division of Pediatric Cardiology
The Children's Hospital of Philadelphia;
Perelman School of Medicine, University of Pennsylvania
Philadelphia, PA USA

Lindsay M. Ryerson MD, FRCPC
Assistant Clinical Professor
University of Alberta;
Division of Pediatric Cardiology
Stollery Children's Hospital
Edmonton, AB, Canada

Craig A. Sable MD
Director, Echocardiography and Telemedicine
Children's National Medical Center
Washington, DC, USA

Ritu Sachdeva MD
Medical Director, Cardiovascular Imaging Research Core
Children's Healthcare of Atlanta Sibley Heart Center;
Associate Professor of Pediatrics
Emory University School of Medicine
Atlanta, GA, USA

Stephen P. Sanders MD
Professor of Pediatrics (Cardiology)
Harvard Medical School;
Director, Cardiac Registry
Departments of Cardiology, Pathology, and Cardiac Surgery
Boston Children's Hospital
Boston, MA, USA

John M. Simpson MD, FRCP, FESC
Consultant in Fetal and Paediatric Cardiology
Department of Congenital Heart Disease
Evelina Children's Hospital;
Guy's and St Thomas' NHS Foundation Trust
London, UK

Timothy C. Slesnick MD
Director of Cardiac MRI
Children's Healthcare of Atlanta Sibley Heart Center;
Assistant Professor of Pediatrics
Emory University School of Medicine
Atlanta, GA, USA

Thierry Sluysmans MD, PhD
Professor of Pediatrics
Université Catholique de Louvain;
Director, Cliniques Universitaires Saint Luc
Brussels, Belgium

Jeffrey F. Smallhorn MBBS, FRACP, FRCPC
Professor of Pediatrics
University of Alberta;
Division of Pediatric Cardiology
Stollery Children's Hospital
Edmonton, AB, Canada

Shubhika Srivastava MBBS
Associate Professor of Pediatrics
Division of Pediatric Cardiology
Mount Sinai Medical Center
New York, NY, USA

Andrew Steer MD
Department of General Medicine and Centre for International Child Health
Department of Paediatrics
Royal Children's Hospital
Melbourne, VIC;
Group A Streptococcal Research Group, Murdoch Childrens Research Institute
Melbourne, VIC, Australia

Cécile Tissot MD
Attending Physician
Pediatric Cardiology Unit
The University Children's Hospital of Geneva
Geneva, Switzerland;
The Heart Institute
Children's Hospital Colorado
Aurora, CO, USA

Anne Marie Valente MD
Associate Professor of Pediatrics and Internal Medicine
Department of Cardiology, Department of Pediatrics
Boston Children's Hospital;
Division of Cardiology, Department of Medicine
Brigham and Women's Hospital;
Harvard Medical School
Boston, MA, USA

Heleen van der Zwaan MD, PhD
Department of Cardiology
Erasmus University Rotterdam
Rotterdam, The Netherlands

Manfred Otto Vogt MD, PhD
Professor of Pediatric Cardiology
Department of Pediatric Cardiology and Congenital Heart Disease
Deutsches Herzzentrum München
Technische Universität München
Munich, Germany

Adel K. Younoszai MD
Associate Professor, University of Colorado Denver
Director of Cardiac Imaging and Fetal Cardiology
The Heart Institute
Children's Hospital Colorado
Aurora, CO, USA

Preface

For the first edition of this textbook, we had set out to fill a void for an updated comprehensive resource on all aspects related to echocardiography in patients with congenital heart disease, from the fetus to the adult. We felt it was important to include detailed information about the anatomy and pathophysiology of each lesion and to describe the goals and techniques of the echocardiographic examinations for diagnosis, guidance of treatment, and monitoring after intervention. In addition to diagrams and still images, hundreds of videos were provided to illustrate key anatomic and functional issues mentioned in the text. We were pleased by the overwhelmingly positive response that the first edition of this book received.

In this second edition, we made improvements in multiple areas. The discussion of fundamental concepts of echocardiography and the sections on imaging techniques were updated to include advances in knowledge and improvements in ultrasound technology. Our coverage of congenital lesions was expanded to include separate chapters on the post-Fontan patient and on pregnancy and heart disease. Each of the lesion chapters now has a section highlighting the *Key elements* of the echocardiogram(s). Finally, all of the figures and videos were reviewed with the goal of upgrading and standardizing image quality and display technique.

The field of echocardiography remains dynamic and constantly evolving. Nevertheless, the mainstay for education in clinical echocardiography continues to be the written text illustrated with images. As we try to expand the resources available to trainees, practitioners, and educators, we are constrained by the publishing format currently available for textbooks. Therefore, our second edition remains mostly accessible in print or PDF format. The videos have moved from being primarily available on DVD to a companion website. Future efforts will no doubt benefit from greater electronic access to the text and images.

As with the first edition, this book is the product of many excellent contributions from the best physician and sonographer experts in the field. We are indebted to their dedication to the field and their commitment to education. We remain grateful to our mentors and colleagues, and we continue to be inspired by our trainees. The staff at Wiley-Blackwell have been truly supportive, and the professional appearance of this book is due to their many contributions. Finally, this and all projects in which the editors are involved remain possible only with the unwavering support of our families and friends.

Wyman W. Lai, MD, MPH
Luc L. Mertens, MD
Meryl S. Cohen, MD
Tal Geva, MD

About the Companion Website

This book is accompanied by a companion website:

www.lai-echo.com

The companion website includes over 580 video clips, referenced at the end of the chapters throughout the book.

PART I

Introduction to Cardiac Ultrasound Imaging

CHAPTER 1

Ultrasound Physics

Jan D'hooge[1] and Luc L. Mertens[2]

[1]Department of Cardiovascular Sciences, Catholic University of Leuven; Medical Imaging Research Center, University Hospital Gasthuisberg, Leuven, Belgium
[2]Cardiology, The Hospital for Sick Children; Department of Pediatrics, University of Toronto, Toronto, ON, Canada

Physics and technology of echocardiography

Echocardiography is the discipline of medicine in which images of the heart are created by using ultrasound waves. Knowledge of the physics of ultrasound helps us to understand how the different ultrasound imaging modalities operate and also is important when operating an ultrasound machine to optimize the image acquisition.

This section describes the essential concepts of how ultrasound waves can be used to generate an image of the heart. Certain technological developments will also be discussed as well as how systems settings influence image characteristics. For more detailed treatment of ultrasound physics and imaging there is dedicated literature, to which readers should refer, for example [1,2].

How the ultrasound image is created

The pulse–echo experiment

To illustrate how ultrasound imaging works, the acoustic "pulse–echo" experiment can be used:

1 A short electric pulse is applied to a piezoelectric crystal. This electric field will induce a shape change of the crystal through reorientation of its polar molecules. In other words, due to application of an electric field the crystal will momentarily deform.
2 The deformation of the piezoelectric crystal induces a local compression of the tissue with which the crystal is in contact: that is, the superficial tissue layer is briefly compressed resulting in an increase in local pressure; this is the so-called acoustic pressure (Figure 1.1).
3 Due to an interplay between tissue elasticity and inertia, this local tissue compression (with subsequent decompression, i.e., rarefaction) will propagate away from the piezoelectric crystal at a speed of approximately 1530 m/s in soft tissue (Figure 1.2). This is called the acoustic wave. The rate of compression/decompression determines the frequency of the wave and is typically 2.5–10 MHz (i.e., 2.5–10 million cycles per second) for diagnostic ultrasonic imaging. As these frequencies cannot be perceived by the human ear, these waves are said to be "ultrasonic." The spatial distance between subsequent compressions is called the wavelength (λ) and relates to the frequency (f) and sound velocity (c) as: $\lambda f = c$. During propagation, acoustic energy is lost mostly as a result of viscosity (i.e., friction) resulting in a reduction in amplitude of the wave with propagation distance. The shorter the wavelength (i.e., the higher the frequency), the faster the particle motion and the larger the viscous effects. Higher frequency waves will thus attenuate more and penetrate less deep into the tissue.
4 Spatial changes in tissue density or tissue elasticity will result in a disturbance of the propagating compression (i.e., acoustic) wave and will cause part of the energy in the wave to be reflected. These so-called "specular reflections" occur, for example, at the interface between different types of tissue (e.g., blood and myocardium) and behave in a similar way to optic waves in that the direction of the reflected wave is determined by the angle between the reflecting surface and the incident wave (cf. reflection of optic waves on a water surface). When the spatial dimensions of the changes in density or compressibility become small relative to the wavelength (i.e., below ~100 μm), these inhomogeneities will cause part of the energy in the wave to be scattered, that is, retransmitted in all possible directions. The part of the scattered energy that is retransmitted back into the direction of origin of the wave is called *backscatter*. Both the specular and backscattered reflections propagate back towards the piezoelectric crystal.
5 When the reflected (compression) waves impinge upon the piezoelectric crystal, the crystal deforms. This results in relative motion of its (polar) molecules and generation of an electric field, which can be detected and measured. The amplitude of this electric signal is directly proportional to the amount of compression of the crystal, that is, the amplitude of the reflected/backscattered wave. This electric signal is called

Echocardiography in Pediatric and Congenital Heart Disease: From Fetus to Adult, Second Edition. Edited by Wyman W. Lai, Luc L. Mertens, Meryl S. Cohen and Tal Geva.

Companion website: www.lai-echo.com

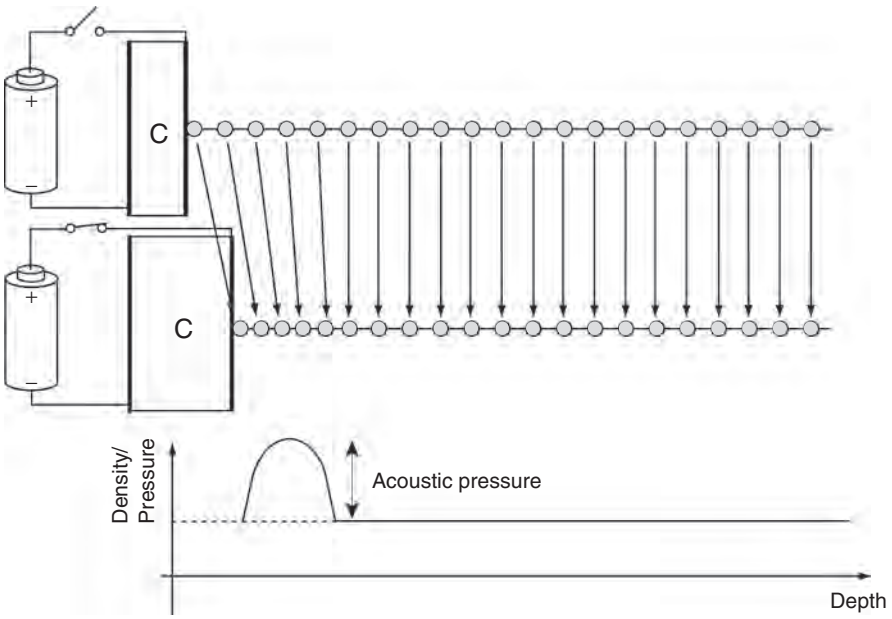

Figure 1.1 Local tissue compression due to deformation of the piezoelectric crystal when applying an electric field.

the radio-frequency (RF) signal and represents the amplitude of the reflected ultrasound wave as a function of time (Figure 1.3). Because reflections occurring further away from the transducer need to propagate further, they will be received later. As such, the time axis in Figure 1.3 can be replaced by the propagation distance of the wave (i.e., depth). The signal detected by the transducer is typically electronically amplified. The amount of amplification has a preset value but can be modified on an ultrasound system by using the "gain" button (typically the largest button on the operating panel). Importantly, the overall gain will amplify both the signal and potential measurement noise and will thus not affect the signal-to-noise ratio.

In the example shown in Figure 1.3, taken from a water tank experiment, two strong specular reflections can be observed (around 50 and 82 μs, respectively) while the lower amplitude reflections in between are scatter reflections. In clinical echocardiography, the most obvious specular reflection is the strong reflection coming from the pericardium observed in the parasternal views as a consequence of its increased stiffness with

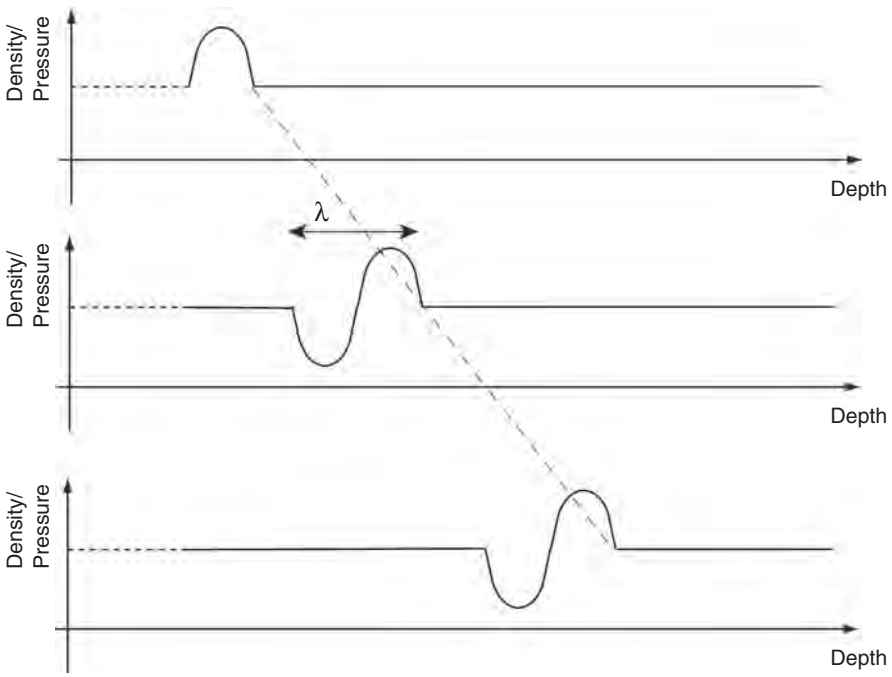

Figure 1.2 The local tissue compression/decompression propagates away from its source at a speed of approximately 1530 m/s in soft tissue.

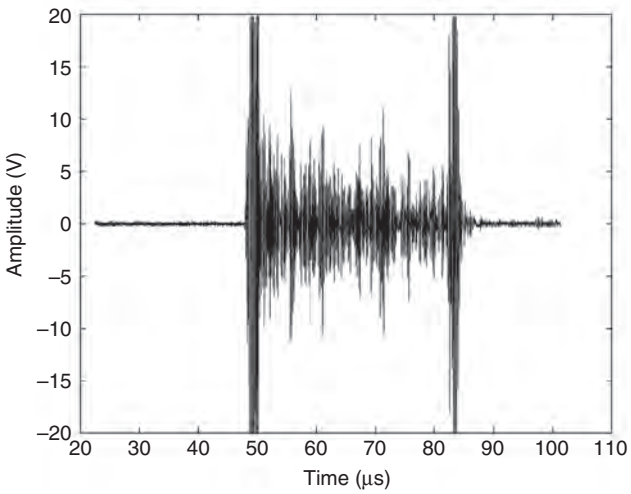

Figure 1.3 The reflected amplitude of the reflected ultrasound waves as a function of time after transmission of the ultrasound pulse is called the radio-frequency (RF) signal.

respect to the surrounding tissues. The direction of propagation of the specular reflection is determined by the angle between the incident wave and the reflecting surface. Thus, the strength of the observed reflection will depend strongly on the exact transducer position and orientation with respect to the pericardium. Indeed, for given transducer positions/orientations, the strong specular reflection might propagate in a direction not detectable by the transducer. For this reason, the pericardium typically does not show as bright in the images taken from an apical transducer position. In contrast, scatter reflections are not angle dependent and will always be visible for a given structure independent of the exact transducer position.

The total duration of the above described "pulse–echo" experiment is about 100 μs when imaging at 5 MHz. The reflected signal in Figure 1.3 is referred to as an A-mode image ("A" referring to "Amplitude") and is the most fundamental form of imaging given that it tells us something about the acoustic characteristics of the materials in front of the transducer. For example, Figure 1.3 clearly shows that at distance of ~3.7 cm in front of the transducer the propagation medium changes density and/or compressibility with a similar change occurring at a distance of ~6.3 cm (these distances correspond to 50/82 μs × 1530 m/s – which is the total propagation distance of the wave – divided by two as the wave has to travel back and forth). The 2.6 cm of material in between these strong reflections is acoustically inhomogeneous (i.e., shows scatter reflections) and thus contains local (very small) fluctuations in mass density and/or compressibility while the regions closer and further away from the transducer do not cause significant scatter and would thus be acoustically homogeneous. Indeed, this A-mode image was taken from a 2.6 cm thick tissue-mimicking material (i.e., gelatin in which small graphite particles were dissolved) put in a water tank.

Grayscale encoding

Since the A-mode image presented above is not visually attractive, the RF signal resulting from a pulse–echo experiment is processed in the following manner:

1 *Envelope detection:* The high-frequency information of the RF signal is removed by detecting the envelope of the signal (Figure 1.4). This process is also referred to as "demodulation."
2 *Grayscale encoding:* The signal is subdivided as a function of time in small intervals (i.e., pixels). Each pixel is attributed a number, defined by the local amplitude of the signal, ranging between 0 and 255 (2^8 or 8-bit image). "0" represents "black;" "255" represents "white;" a value in between is represented by a grayscale. By definition, bright pixels correspond to high-amplitude reflections. This process is illustrated in Figure 1.4. Please note that a different kind of color encoding is also possible simply by attributing different colors to the range of values between 0 and 255. For example, shades of blue or bronze are also popularly used. The choice of the color map used to display an image is a matter of preference and can easily be changed on all ultrasound systems. Nowadays, most ultrasound systems have 12- or 16-bit resolution images (i.e., encoding 4096 or 65536 gray/color levels).
3 *Attenuation correction*: As wave amplitude decreases with propagation distance due to attenuation (mostly due to conversion of acoustic energy to heat), reflections from deeper structures are intrinsically smaller in amplitude and therefore show less bright. In order to give identical structures located at different distances from the transducer a similar gray value (i.e., reflected amplitude), compensation for this attenuation must occur. Thus, an attenuation profile as a function of distance from the transducer is assumed, which allows for automatic amplification of the signals from deeper regions – the so-called *automated* time-gain compensation (TGC), also referred to as depth-gain compensation. As the pre-assumed attenuation profile might be incorrect, sliders on the ultrasound scanner (TGC toggles) allow for manual correction of the automatic compensation and will result in more or less local amplification of the received signal as required to obtain a more homogenous brightness of the image. In this way, the operator can optimize local image brightness. It is recommended to start scanning using a neutral setting of these sliders, as attenuation characteristics will be patient and view specific. For each view the TGC can be optimized manually.
4 *Log-compression*: In order to increase the image contrast in the darker (i.e., less bright) regions of the image, gray values in the image may be redistributed according to a logarithmic curve (Figure 1.5). The characteristics of this compression (i.e., local contrast enhancement) can be changed through settings on the ultrasound scanner. They will not change the ultrasound acquisition as such (and thus impact image quality) but will merely influence the visual representation of the resulting image. This is similar to what is nowadays very common in digital photography, where ambient lighting

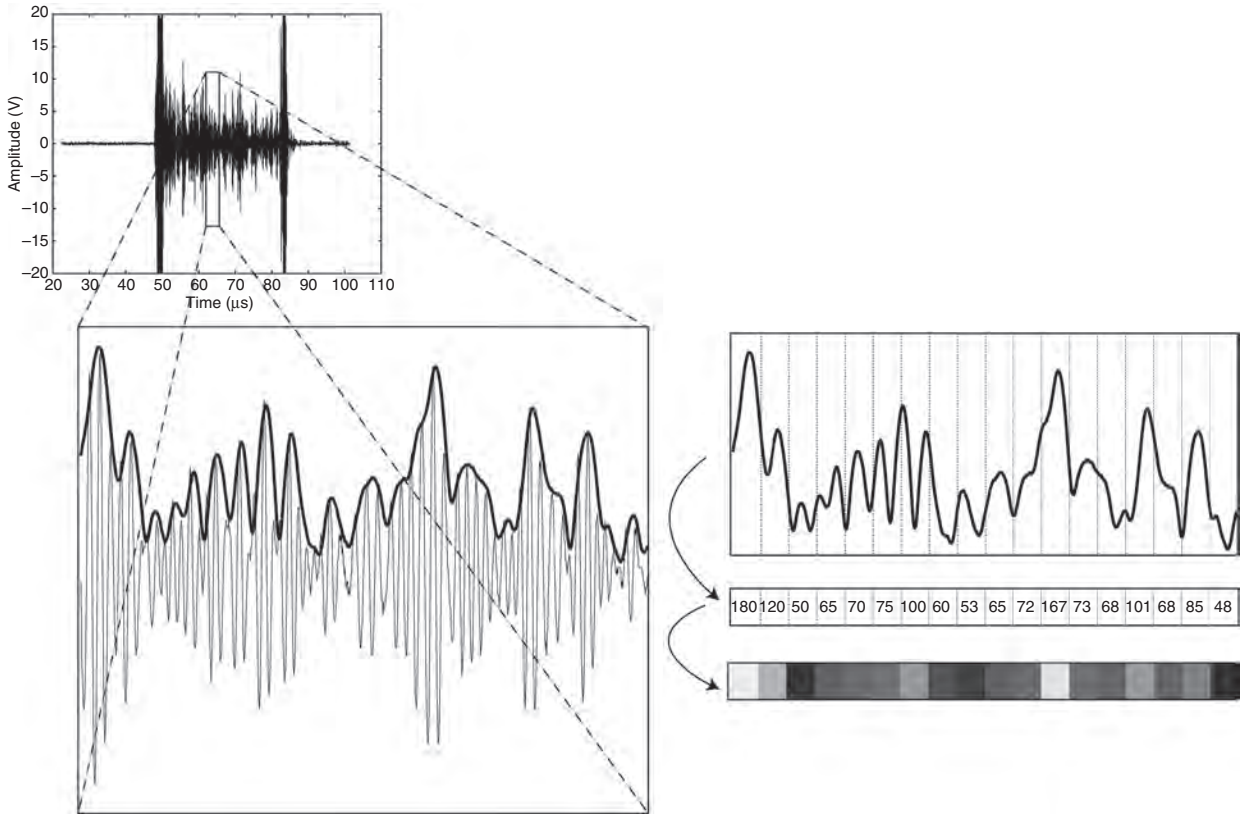

Figure 1.4 The RF signal is demodulated in order to detect its envelope. This envelope signal (bold) is color encoded based on the local signal amplitude.

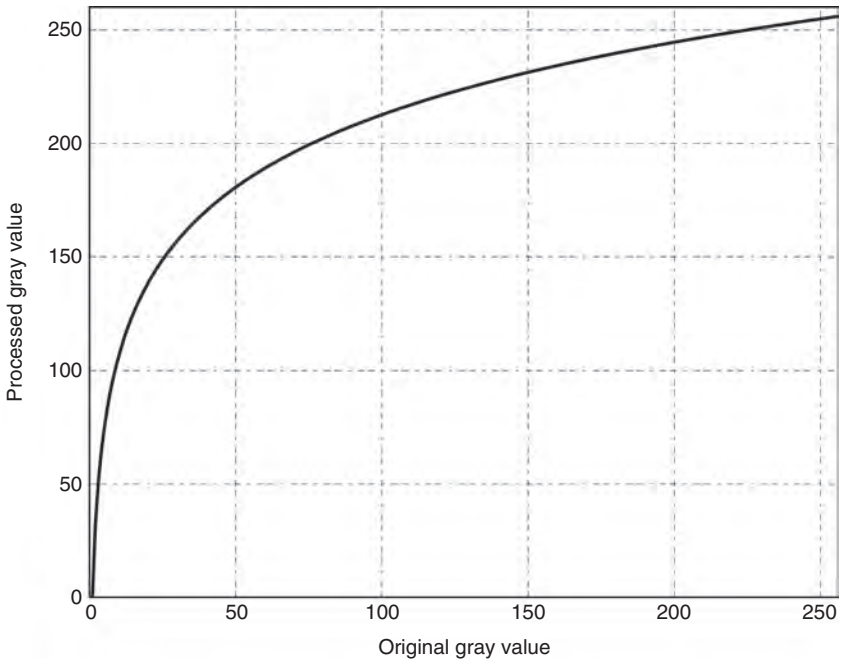

Figure 1.5 The logarithmic compression curve.

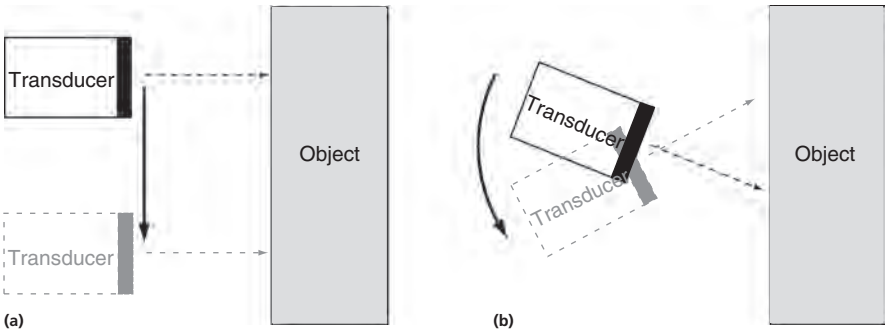

Figure 1.6 Translation of the ultrasound source results in a linear image format **(a)** whereas pivoting results in sector images **(b)**.

and/or contrast can be retrospectively enhanced. The setting on the system impacting the visual aspect of the image is the so-called "dynamic range" which will change the number of gray values used and will therefore result in "hard" (i.e., almost black-and-white images without much gray) or "soft" images for low and high dynamic range, respectively.

Image construction

In order to obtain an ultrasound image, the above procedures of signal acquisition and post-processing are repeated.

For conventional B-mode imaging ("B" referring to "brightness" mode), the transducer can either be translated (Figure 1.6a) or tilted (Figure 1.6b) within a plane between two subsequent "pulse–echo" experiments. In this way, a conventional 2D cross-sectional image is obtained. The same principle holds for 3D imaging by moving the ultrasound beam in 3D space between subsequent acquisitions.

Alternatively, the ultrasound beam is transmitted into the same direction for each transmitted pulse. In that case, an image line is obtained as a function of time, which is particularly useful to look at motion. This modality is therefore referred to as M-mode (motion-mode) imaging.

Image artifacts

Side lobe artifacts

In the construction of an ultrasound image, the assumption is made that all reflections originate from a region directly in front of the transducer. Although most of the ultrasound energy is indeed centered on an axis in front of the transducer, in practice part of the energy is also directed sideways (i.e., directed off-axis). The former part of the ultrasound beam is called the main lobe whereas the latter is referred to as the side lobes (Figure 1.7).

Because the reflections originating from these side lobes are much smaller in amplitude than the ones coming from the main lobe, they can typically be neglected. However, image artifacts can arise when the main lobe is in an anechoic region (i.e., a cyst or inside the left ventricular cavity) causing the relative contribution of the side lobes to become significant. In this way, a small cyst or lesion may be more difficult to detect, as it appears brighter than it should due to spillover of (side-lobe) energy from neighboring regions. Similarly, when using contrast agents (see later) the reflections resulting from small side lobes may still become significant as these agents reflect energy strongly. As such, increased brightness may appear in regions adjacent to regions filled with contrast without contrast being present in the region itself.

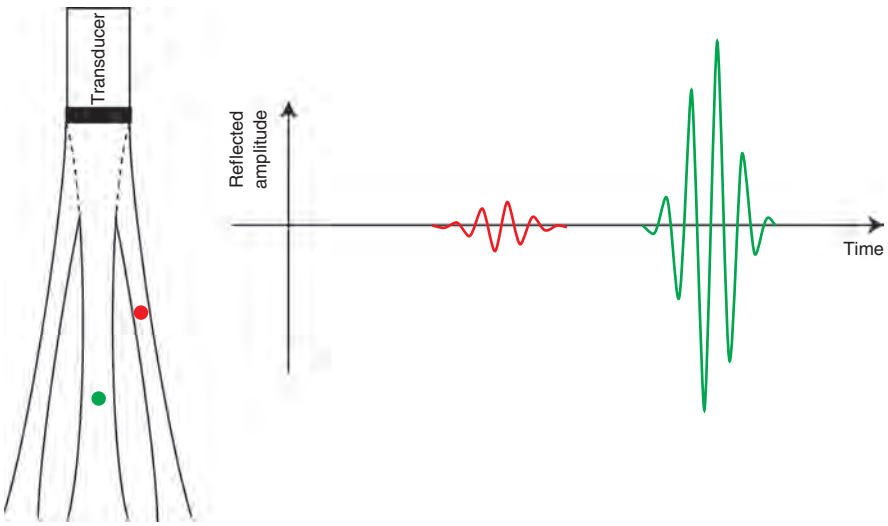

Figure 1.7 Reflections caused by side lobes (red) will induce image artifacts because all reflections are assumed to arrive from the main ultrasound lobe (green).

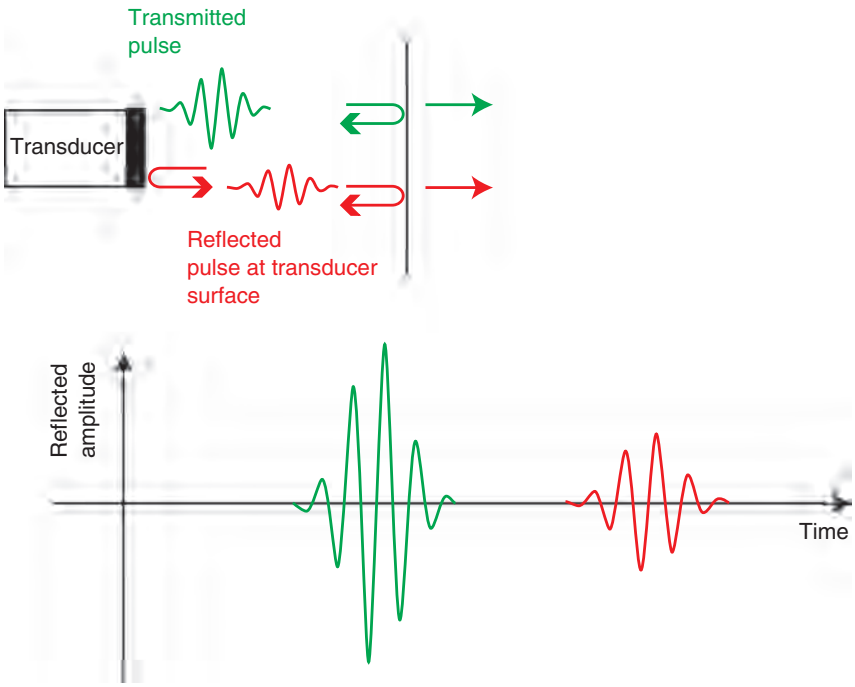

Figure 1.8 A transmitted wave (green) will reflect and result in an echo signal (green). The reflected wave will, however, partially reflect at the transducer surface (red) and generate secondary signals (red).

Reverberation artifacts

When the reflected wave arrives at the transducer, part of the energy is converted to electrical energy as described in the previous section. However, another part of the wave is simply reflected on the transducer surface and will start propagating away from the transducer as if it were another ultrasound transmission. This secondary "transmission" will propagate in a way similar to that of the original pulse, which means that it is reflected by the tissue and detected again (Figure 1.8).

These higher-order reflections are called reverberations and give rise to ghost (mirror image) structures in the image. These ghost images typically occur when strongly reflecting structures such as ribs or the pericardium are present in the image. Similarly, as the reflected wave coming from the pericardium is very strong, its backscatter (i.e., propagating again towards the pericardium) will be sufficiently strong as well. This wave will reflect on the pericardium and can be detected by the transducer after the actual pericardial reflection arrives. In clinical practice, this causes a ghost image to be created behind the pericardial reflection that typically appears as a mirror image of the left ventricle around the pericardium in a parasternal long-axis view.

Shadowing and dropout artifacts

When perfect reflections occur, no acoustic energy is transmitted to more distal structures and – as a consequence – no reflections from these distal structures can be obtained. As a result, a very bright structure will appear in the image followed by a signal void, that is, an acoustic shadow. For example, when a metallic artificial valve has been implanted, the metal (being very dense and extremely stiff) can cause close to perfect ultrasound reflections resulting in an apparently anechoic region distal to the valve. This occurs because no ultrasound energy reaches these deeper regions. Similarly, some regions in the image may receive little ultrasound energy due to superficial structures blocking ultrasound penetration. Commonly, ribs (being more dense and stiff than soft tissue) are fairly strong reflectors at cardiac diagnostic frequencies and can impair proper visualization of some regions of the image. These artifacts are most commonly referred to as "dropout" and can only be avoided – if at all – by changing the transducer position/orientation.

When signal dropout occurs at deeper regions only, the acoustic power transmitted can be increased. This will obviously result in more energy penetrating to deeper regions and will increase the overall signal-to-noise ratio of the image (in contrast to increasing the overall gain of the received signals as explained earlier). However, the maximal transmit power allowed is limited in order to avoid potential adverse biological effects. Indeed, at higher energy levels, ultrasound waves can cause tissue damage either due to cavitation (i.e., the formation of vapor cavities that subsequently implode and generate very high local pressures and temperatures) or tissue heating. The former risk is quantified in the "mechanical index" (MI) and should not pass a value of 1.9 while the latter is estimated through a "thermal index" (TI). Both parameters are displayed on the monitor during scanning and will increase with increasing power output. The operator thus has to find a compromise between image quality (including penetration depth) and the risk of adverse biological effects. In case penetration is not appropriate at maximal transmit power, the operator has to choose a transducer with lower transmit frequency (see earlier).

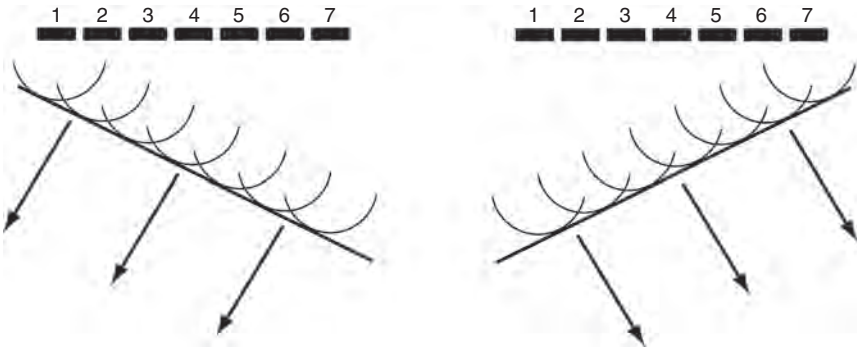

Figure 1.9 An array of crystals can be used to steer the ultrasound beam electronically by introducing time delays between the activation of individual elements in the array.

Ultrasound technology and image characteristics

Ultrasound technology

Phased array transducers

Rather than mechanically moving or tilting the transducers, as in early generation ultrasound machines, modern ultrasound devices use electronic beam steering. To do this an array of piezoelectric crystals is used. By introducing time delays between the excitation of different crystals in the array, the ultrasound wave can be sent in a specific direction without mechanical motion of the transducer (Figure 1.9). The RF signal for a transmission in a particular direction is then simply the sum of the signals received by the individual elements. These individual contributions can be filtered, scaled, and time-delayed separately before summing. This process is referred to as *beam-forming* and is a crucial element for obtaining high-quality images. The scaling of the individual contributions is typically referred to as *apodization* and is critical in suppressing side lobes and thus avoiding the associated artifacts.

This concept can be generalized by creating a 2D matrix of elements that enables steering of the ultrasound beam in three dimensions. This type of transducer is referred to as a matrix array or 2D array transducer. Because each of the individual elements of such an array needs electrical wiring, manufacturing such a 2D array remained technically challenging for many years, in part because of the limitation of the thickness of the transducer cable. Generally, these obstacles have been overcome and 2D arrays are now readily available.

Second harmonic imaging

Wave propagation as illustrated in Figure 1.2 is only valid when the amplitude of the ultrasound wave is relatively small (i.e., the acoustic pressures involved are small). Indeed, when the amplitude of the transmitted wave becomes significant, the shape of the ultrasound wave will change during propagation, as illustrated in Figure 1.10. This phenomenon of wave distortion during propagation is referred to as nonlinear wave propagation. It can be shown that this wave distortion causes harmonic frequencies (i.e., integer multiples of the transmitted frequency) to be

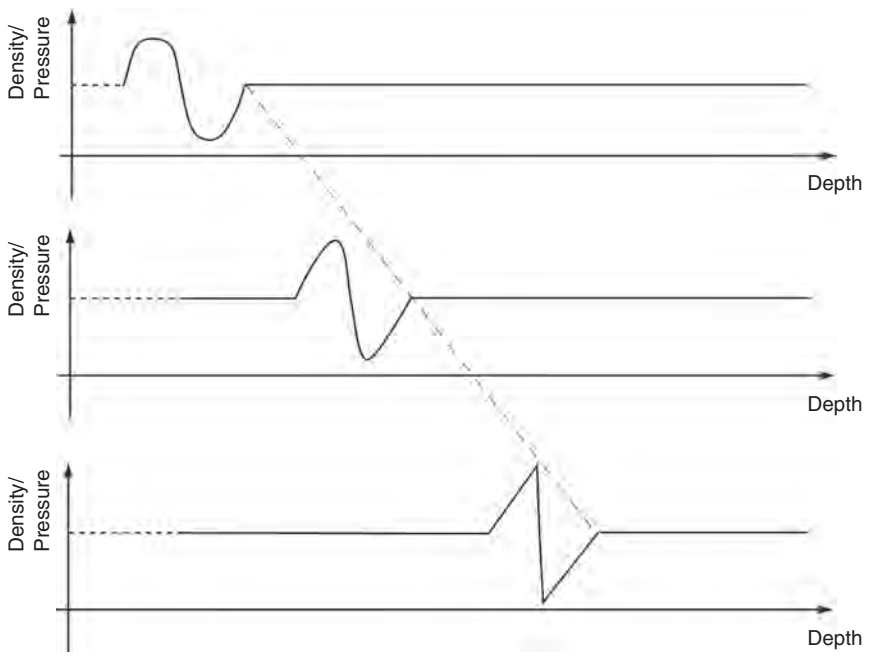

Figure 1.10 Nonlinear wave behavior results in changes in shape of the waveform during propagation.

generated. Transmitting a 1.7-MHz ultrasound pulse will thus result in the spontaneous generation of frequency components of 3.4, 5.1, 6.8, 8.5 MHz, and so on. These harmonic components will grow stronger with propagation distance. The rate at which the waveform distorts for a specific wave amplitude is tissue dependent and characterized by a nonlinearity parameter, β (or the so-called "B/A" parameter).

The ultrasound scanner can be set up to receive only the second harmonic component through filtering of the received RF signal. If further post-processing of the RF signal is done in exactly the same way as described earlier, a second harmonic image is obtained. Such an image typically has a better signal-to-noise ratio by avoiding clutter noise due to (rib) reverberation artifacts. This harmonic image is commonly used in patients with poor acoustic windows and poor penetration. Although harmonic imaging increases signal-to-noise, it has intrinsically poorer axial resolution as elucidated later. Please note that higher harmonics (i.e., third, fourth, etc.) are present but typically fall outside the bandwidth of the transducer and thus remain undetected. Harmonic imaging has become the default cardiac imaging mode for adult scanning on many systems. It is typically unnecessary to use harmonic imaging in young infants but is often required to enhance the image in the older patient. Switching between conventional and harmonic imaging is done by changing the transmit frequency of the system. For lower frequency transmits, it will automatically enter a harmonic imaging mode, which is indicated on the display by showing both transmit and receive frequencies (i.e., 1.7/3.4 MHz). When a single frequency is displayed, the scanner is in a conventional (i.e., fundamental) imaging mode. For pediatric scanning, especially in smaller infants, fundamental imaging is the preferred mode due to its better spatial resolution.

Contrast imaging

As blood reflects little ultrasound energy it shows dark in the image. For some applications (such as myocardial perfusion assessment) it can be useful to artificially increase the blood reflectivity. This can be achieved using an ultrasound contrast agent. As air is an almost perfect reflector of ultrasound energy given it is very compressible and has a low density compared to soft tissue, it often is used as a contrast agent. As such, the injection of small air bubbles (of diameter similar to that of red blood cells) will increase blood reflectivity. This can be done using agitated saline or by using ultrasound contrast agents that encapsulate air bubbles in order to limit diffusion of the air (or a heavier gas) in blood. Contrast imaging can be used to help in visualizing the endocardial border by enhancing the difference in gray value between the myocardium and the blood pool (i.e., left ventricular opacification) or to detect shunts. Similarly, contrast agents can be used to increase the brightness of perfused (myocardial) tissue although artifacts become more prominent and may make interpretation less obvious. At present, different contrast agents are commercially available for clinical use but none of them have been approved for pediatric use. Especially in the presence of right-to-left shunting, contrast agents should be used carefully.

Image resolution

Resolution is defined as the shortest distance at which two adjacent objects can be distinguished as separate. The spatial resolution of an ultrasound image varies depending on the position of the object relative to the transducer. Also the resolution in the direction of the image line (range or *axial* resolution) is different from the one perpendicular to the image line within the 2D image plane (azimuth or *lateral resolution*), which is different again from the resolution in the direction perpendicular to the image plane (*elevation resolution*).

Axial resolution

In order to obtain an optimal axial resolution, a short ultrasound pulse needs to be transmitted. The length of the transmitted pulse is mainly determined by the characteristics of the transducer. Current transducers can generate multiple frequencies influencing axial resolution by selecting different frequencies. The bandwidth is most commonly expressed relative to the center frequency of the transducer. A typical value would be 80% implying that for a 5-MHz transducer the absolute bandwidth is about 4 MHz. This type of transducer can thus generate/receive frequencies in the range of 3–7 MHz. The absolute transducer bandwidth is typically proportional to the mean transmission frequency. A higher frequency transducer will thus produce shorter ultrasound pulses and thus, better axial resolution. Unfortunately, higher frequencies are attenuated more by soft tissue and are impacted by depth (see earlier). As such, a compromise needs to be made between image resolution and penetration depth (i.e., field of view). In pediatric and neonatal cardiology, higher frequency transducers can be used that increase image spatial resolution. Generally, for infants 10–12-MHz transducers are used resulting in a typical axial resolution of the order of 250 μm.

Most systems allow changing the transmit frequency of the ultrasound pulse within the bandwidth of the transducer. As such, a 5-MHz transducer can be used to transmit a 3.5-MHz pulse which can be practical when penetration is not sufficient at 5 MHz. The lower frequency will result in a longer transmit pulse with a negative impact on axial resolution. Similarly, for second harmonic imaging a narrower band pulse needs to be transmitted, as part of the bandwidth of the transducer needs to be used to be able to receive the second harmonic. As such, in harmonic imaging mode, a longer ultrasound pulse is transmitted (i.e., less broadband) resulting in a worse axial resolution of the second harmonic image despite improvement of the signal-to-noise ratio. Therefore, some of the cardiac structures appear thicker, especially valve leaflets. This should be considered when interpreting the images.

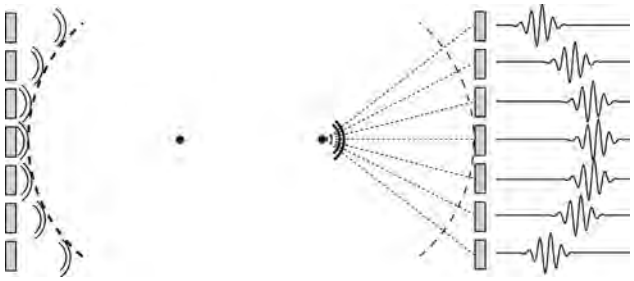

Figure 1.11 Introducing time delays during transmission of individual array elements (left) allows for all wavelets to arrive at a particular point (focus) simultaneously. Similarly, received echo signals can be time delayed so that they constructively interfere (receive focus).

Lateral resolution

Lateral resolution is determined by the width of the ultrasound beam (i.e., the width of the main lobe). The narrower the ultrasound beam, the better the lateral resolution. In order to narrow the ultrasound beam, several methods can be used but the most obvious one is focusing. This is achieved by introducing time delays between the firing of individual array elements (similar to what is done for beam steering) in order to assure that the transmitted wavelets of all individual array elements arrive at the same position at the same time and will thus constructively interfere (Figure 1.11). Similarly, time delaying the reflections of the individual crystals in the array will make sure that reflections coming from a particular point in front of the transducer will sum in phase and therefore create a strong echo signal (Figure 1.11). Because the sound velocity in soft tissue is known, the position from which reflections can be expected is known at each time instance after transmission of the ultrasound pulse. As such, the time delays applied in receive can be changed dynamically in order to move the focus point to the appropriate position. This process is referred to as *dynamic (receive) focusing*. In practice, dynamic receive focusing is always used and does not need adjustments by the operator in contrast to the transmit focus point whose position should be set manually. Obviously, to resolve most morphologic detail, the transmit focus should always be positioned close to the structure/region of interest. Most ultrasound systems allow selecting multiple transmit focal points. In this setting, each image line will be created multiple times with a transmit pulse at each of the set focus positions and the resulting echo signals will be combined in order to generate a single line in the image. Although this results in a more homogeneous distribution of the lateral resolution with depth, this obviously implies that it takes more time to generate a single image and thus will result in lowering the frame rate (i.e., temporal resolution).

The easiest way to improve the focus performance of a transducer is by increasing its size (i.e., aperture). Unfortunately, the footprint needs to fit between the patient's ribs, thereby limiting the size of the transducer and thus limiting lateral resolution of the imaging system. For an 8-MHz pediatric transducer, realistic numbers for the lateral resolution of the system are depth dependent and are approximately 0.3 mm at 2 cm going up to 1.2 mm at 7 cm depth.

Elevation resolution

For elevation resolution, the same principles hold as for lateral resolution in the sense that the dimension of the ultrasound beam in the elevation direction will be determinant. However, most ultrasound devices are still equipped with 1D array transducers. As such, focusing in the elevation direction needs to be done by the use of acoustic lenses (similar to optic lenses acoustic lenses concentrate energy in a given spatial position), which implies that the focus point is fixed in both transmit and receive (i.e., dynamic focusing is not possible in the elevation direction). This results in a resolution in the elevation direction that is worse than the lateral resolution. The homogeneity of the resolution is also worse with depth. Moreover, transducer aperture in the elevation direction is typically somewhat smaller (in order to fit in between the ribs of the patient) resulting in a further decrease of elevation resolution compared to the lateral component. Newer systems with 2D array transducer technology have more similar lateral and elevation image resolution. Matrix array transducers not only create 3D images but also allow generating 2D images of higher/more homogeneous spatial resolution.

Temporal resolution

Typically, a 2D pediatric cardiac image consists of 300 lines. The construction of a single image thus takes about 300 × 100 μs (the time required to acquire one line as explained earlier) or 30 ms. About 33 images can be produced per second, which is sufficient to look at motion (e.g., standard television displays only 25 frames per second). With more advanced imaging techniques such as parallel beam forming, higher frame rates can be obtained (70–80 Hz). In order to increase frame rate, either the field of view can be reduced (i.e., a smaller sector will require fewer image lines to be formed and will thus speed up the acquisition of a single frame) or the number of lines per frame (i.e., the line density) can be reduced. The latter comes at the cost of spatial resolution, as image lines will be further apart. There is thus an intrinsic trade-off between the image field-of-view, spatial resolution and temporal resolution. Most systems have a "frame rate" button nowadays that allow changing the frame rate although this always comes at the expense of spatial resolution. Higher frame rates are important when the heart rate is higher as is often the case in pediatric patients and when you want to study quickly moving structures like valve leaflets or myocardial wall motion.

Image optimization in pediatric echocardiography

All the aforementioned principles can be used to optimize image acquisition in the pediatric population. As children are smaller, less penetration is required. The heart rates are higher